THE JOURNAL OF PHYSICAL CHEMISTRY A

ARTICLE

pubs.acs.org/JPCA

TD-CI Simulation of the Electronic Optical Response of Molecules in Intense Fields: Comparison of RPA, CIS, CIS(D), and EOM-CCSD

Jason A. Sonk,[†] Marco Caricato,[‡] and H. Bernhard Schlegel*[,†]

[†]Department of Chemistry, Wayne State University, Detroit, Michigan 48202, United States

[‡]Gaussian, Inc., 340 Quinnipiac Street, Building 40, Wallingford, Connecticut 06492, United States

ABSTRACT: A number of different levels of theory have been tested in TD-CI simulations of the response of butadiene interacting with very short, intense laser pulses. Excitation energies and transition dipoles were calculated with linear-response time-dependent Hartree−Fock (also known as the random phase approximation, RPA), configuration interaction in the space of single excitations (CIS), perturbative corrections to CIS involving double excitations [CIS(D)], and the equation-of-motion coupled-cluster (EOM-CC) method using the 6-31G(d,p) basis set augmented with n = 0−3 sets of diffuse sp functions on all carbons and only on the end carbons [6-31 n+G(d,p) and 6-31(n+)G(d,p), respectively]. Diffuse functions are particularly important for transitions between the pseudocontinuum states above the ionization threshold. Simulations were carried out with a three-cycle Gaussian pulse (ω = 0.06 au, 760 nm) with intensities up to 1.26 × 10^{14} W cm^{-2} directed along the vector connecting the end carbons. Depending on the basis set, up to 500 excited states were needed for the simulations. Under the conditions selected, the response was too weak with the 6-31G(d,p) basis set, and the difference between levels of theory was more pronounced. When two or three set of diffuse functions were included on all of the carbons, the RPA, CIS, and EOM-CC results were comparable, but the CIS(D) response was too large compared to the more accurate EOM-CC calculations. Even though the frequency of the pulse is not resonant with any of the ground-to-excited transitions, excitations to valence and pseudocontinuum states occur readily above a threshold in the intensity.

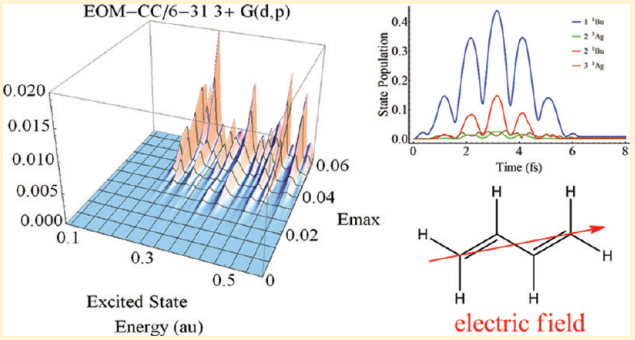

INTRODUCTION

When molecules are subjected to short, intense femtosecond and picosecond laser pulses, a variety of strong-field effects are observed.[1−12] These effects include field tunneling and barrier-suppression ionization, above-threshold ionization, field-induced resonant enhancement of electronic absorption, nonadiabatic multielectron excitation, and generation of higher-order harmonic emissions. Recent advances using higher harmonics generated by short intense pulses include imaging molecular orbitals, following chemical processes on a femtosecond time scale, and probing the detailed dynamics of ionization.[8,13−24] The strong-field response of a molecule cannot be treated by perturbative methods when the electric field of the laser is comparable with that sampled by valence electrons. Under these circumstances, the behavior of the electronic density interacting with intense electric fields has to be simulated by numerical methods. For few-electron systems, accurate simulation methods are available;[25−46] however, these cannot be applied to larger polyatomic systems of interest in strong-field chemistry. In the present article, we examine a few of the approximate methods that can be used to simulate some aspects of these processes in molecules.

Atomic systems have been studied extensively, and accurate results are available for very simple molecules such as H_2^+ and H_2.[25−46] For larger, many-electron systems, some approximations are needed. Chu and co-workers[47−53] studied many-electron atoms and diatomics using time-dependent generalized pseudospectral methods, self-interaction-corrected density functional theory, and Floquet matrix techniques. Greenman et al.[54] used TD-CIS with grid based orbitals for many electron atoms. Suzuki and Mukamel[55,56] simulated π-electron dynamics in octatetraene with a semiempirical Hamiltonian and modeled ionization saturation intensities in a multielectron system in a finite one-dimensional box. Cederbaum and collaborators[57−62] and Levine and co-workers[63−69] used a multielectron wavepacket dynamics approach to investigate hole migration following ionization. Klamroth and co-workers[70−74] used optimal control theory and time-dependent configuration interaction with single excitations (TD-CIS) to shape short, intense pulses for state-selective excitation of N-methylquinoline and employed

Received: August 5, 2010
Revised: March 22, 2011
Published: April 15, 2011

TD-CIS(D) to simulate dipole switching in lithium cyanide. They also used heuristic methods to include the effects of ionization, dissipation, and dephasing.[75−77] Li and co-workers combined real-time integration of time-dependent density functional theory with Ehrenfest dynamics to investigate laser-controlled dissociation processes.[78−80] In previous works, we used TD-HF (time-dependent Hartree−Fock) and TD-CIS methods to simulate the response of CO_2, polyenes, and polyacenes and their cations to short, intense laser pulses.[81−86] The approximate simulations that have been carried out to date on polyatomic systems are promising, but there is a need to compare the performance of the various methods.

Practical calculations on polyatomic systems require some compromises between efficiency and accuracy. Real-time response TD-HF and TD-CIS are the least expensive methods available for larger systems, but they do not include multielectron excitations. CIS(D) treats the effects of higher excitations perturbatively, whereas CISD includes double excitations explicitly. The equation-of-motion coupled-cluster (EOM-CC) method accounts for electron correlation effects as well as higher excitations. The EOM-CC approach is considered to be the method of choice for systems that are too large for extensive multireference configuration interaction calculations. Practical calculations are also limited in the numbers of basis functions and excited states that can be considered in the simulations. In the present work, we test TD-CI methods for simulating the evolution of the electron density of butadiene during a short, intense laser pulse and just prior to ionization. Ionization was not studied in this work but could be simulated by applying appropriate absorbing boundary conditions to the pseudocontinuum states.[77] In this work, we focus on comparing the performance of TD-CI simulations with different numbers of excited states calculated using linear-response TD-HF or RPA, CIS, CIS(D), and EOM-CCSD with various basis sets. The present work will serve as a benchmark for our study comparing the performance of various density functional methods in TD-CI simulations of molecules in strong fields.

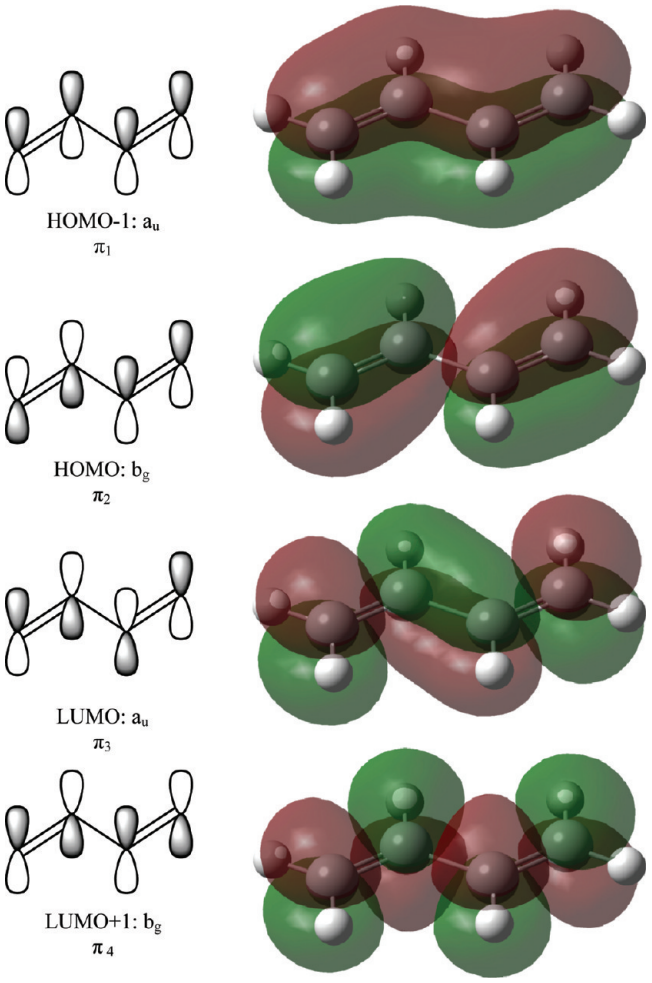

Figure 1. Highest occupied and lowest unoccupied π molecular orbitals of 1,3-butadiene calculated by HF/6-31G(d,p).

METHODS

The time-dependent Schrödinger equation (TDSE) in atomic units is

$$i\frac{d\psi(t)}{dt} = \hat{H}(t)\,\psi(t) \tag{1}$$

The wave function can be expanded in terms of the ground state $|\varphi_0\rangle$ and excited states $|\varphi_i\rangle$ of the time-independent, field-free Hamiltonian

$$\psi(t) = \sum_{i=0} C_i(t)|\varphi_i\rangle \tag{2}$$

An excited state, φ_i ($i > 0$), can be written in terms of an excitation operator, $\hat{R}_i$, acting on the reference determinant φ_0

$$|\varphi_i\rangle = \hat{R}_i|\varphi_0\rangle, \quad \hat{R}_i = \sum r_0 + r_i^a \hat{a}^\dagger\hat{i} + r_{ij}^{ab}\hat{a}^\dagger\hat{i}\hat{b}^\dagger\hat{j}\cdots \tag{3}$$

The excitation operator involves amplitudes, r, and creation and annihilation operators to generate single, double, and higher excitations by promoting electrons from occupied orbitals ijk to unoccupied orbitals abc. For configuration interaction calculations (CIS, CISD, etc.), the amplitudes and excitation energies are obtained by diagonalizing the corresponding field-free Hamiltonian matrix of the time-independent Schrödinger equation

$$\hat{H}_0|\varphi_i\rangle = \omega_i|\varphi_i\rangle, \quad \langle\varphi_i|\varphi_j\rangle = \delta_{ij} \tag{4}$$

The excitation energies can also be obtained by linear-response time-dependent Hartree−Fock theory, also known as the random phase approximation (RPA).

In the coupled-cluster approach with single and double excitations (CCSD), the ground state is given by the exponential coupled-cluster operator acting on the reference determinant

$$|\varphi_0\rangle^{\mathrm{CCSD}} = \exp(\hat{T})|\varphi_0\rangle, \quad \hat{T} = \sum t_i^a \hat{a}^\dagger\hat{i} + t_{ij}^{ab}\hat{a}^\dagger\hat{i}\hat{b}^\dagger\hat{j} \tag{5}$$

Excited states in the equation-of-motion coupled-cluster method are written in terms of the excitation operator acting on the coupled-cluster ground state

$$|\varphi_i\rangle^{\mathrm{EOMCC}} = \hat{R}_i \exp(\hat{T})|\varphi_0\rangle \tag{6}$$

Because the $\hat{R}$ and $\hat{T}$ operators commute, the amplitudes for the excitation operator can be obtained by solving for the eigenvalues

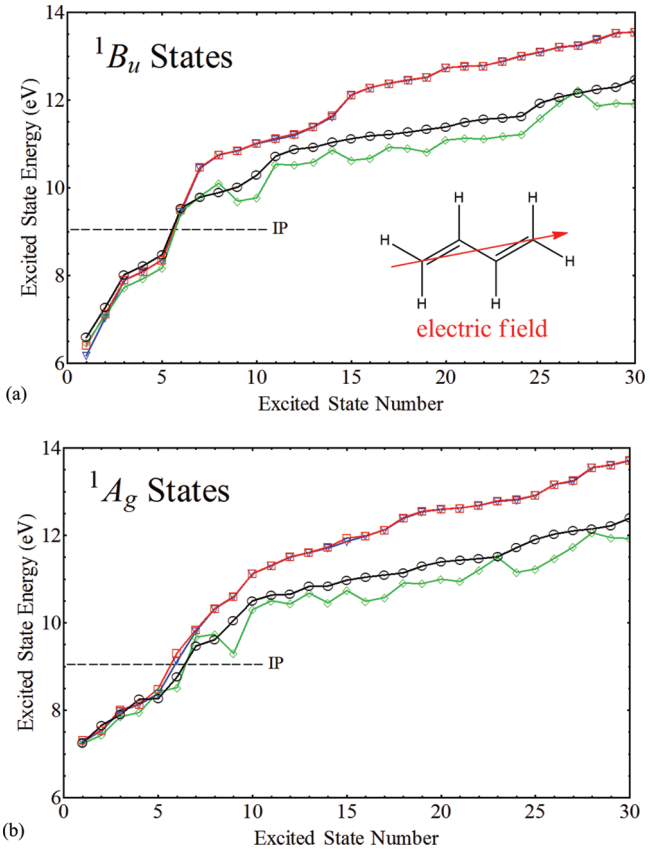

Figure 2. Vertical excitation energies of butadiene for the first 30 ^1B_u and ^1A_g states calculated with the 6-31 3+ G(d,p) basis set [RPA (blue triangles), CIS (red squares), CIS(D) (green diamonds), EOM-CC (black circles)]. IP is the experimentally determined ionization potential.[91]

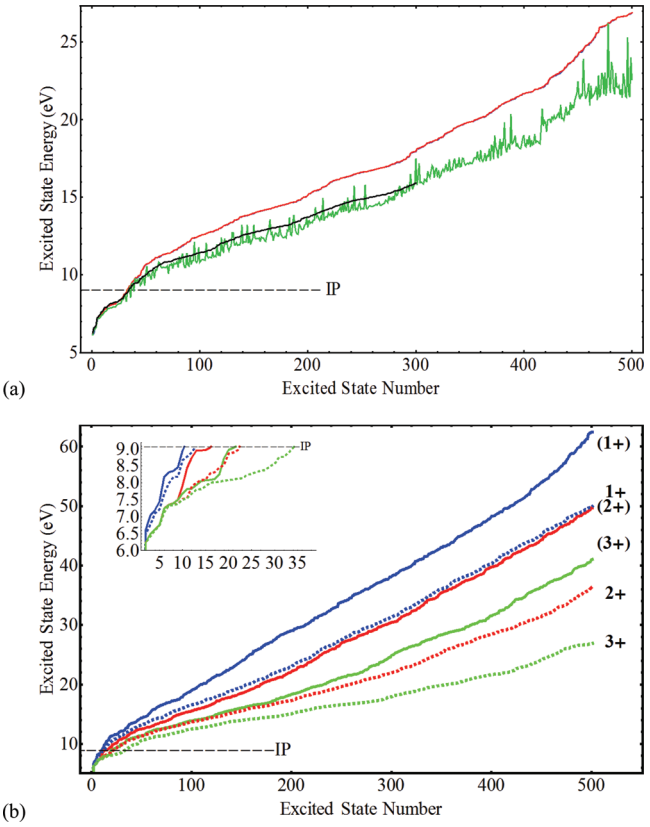

Figure 3. Vertical excitation energies for the first 500 states of butadiene (all symmetries) calculated with (a) the 6-31 3+ G(d,p) basis and RPA, CIS, CIS(D), and EOM-CC (blue, red, green, and black, respectively); (b) CIS and the 6-31 n+ G(d,p) and 6-31(n+)G(d,p) basis sets [n = 1, blue; n = 2, red; n = 3, green; solid lines, (n+); dotted lines, n+]. Inset: Number of states under the experimental ionization potential.[91]

of the similarity transformed field-free Hamiltonian, $\bar{H}_0$

$$\hat{H}_0\hat{R}_i \exp(\hat{T})|\varphi_0\rangle = \omega_i\hat{R}_i \exp(\hat{T})|\varphi_0\rangle$$
$$\bar{H}_0\hat{R}_i|\varphi_0\rangle = \omega_i\hat{R}_i|\varphi_0\rangle$$
$$\bar{H}_0 = \exp(-\hat{T})\hat{H}_0 \exp(\hat{T}) \quad (7)$$

Because $\bar{H}_0$ is not Hermitian, there is also a set of left-hand eigenstates that satisfies the property of biorthogonality

$$\langle\varphi_0|\hat{L}_i\bar{H}_0 = \langle\varphi_0|\hat{L}_i\omega_i, \quad \langle\varphi_0|\hat{L}_i\bar{H}_0\hat{R}_j|\varphi_0\rangle = \omega_i\delta_{ij} \quad (8)$$

Inserting eq 2 into eq 1 and multiplying from the left by $\langle\varphi_i|$ reduces the time-dependent Schrödinger equation to a set of coupled differential equations for the time-dependent coefficients

$$i\frac{dC_i(t)}{dt} = \sum_j H_{ij}(t)\, C_j(t) \quad (9)$$

This expression can be integrated numerically using a unitary transform approach

$$\mathbf{C}(t+\Delta t) = \exp[-i\mathbf{H}(t+\Delta t/2)\Delta t]\mathbf{C}(t) \quad (10)$$

In the dipole approximation, the matrix elements of the field-dependent Hamiltonian in eqs 9 and 10 can be expressed in terms of the field-free energies, ω_i; transition dipole moments, $\mathbf{D}_{ij}$; and the electric field, $\mathbf{e}(t)$, as

$$H_{ij}(t) = \langle\varphi_i|\hat{H}(t)|\varphi_j\rangle = \langle\varphi_i|\hat{H}_0|\varphi_j\rangle + \langle\varphi_i|\hat{r}|\varphi_j\rangle\cdot\mathbf{e}(t)$$
$$= \omega_i\delta_{ij} + \mathbf{D}_{ij}\cdot\mathbf{e}(t) \quad (11)$$

For CIS(D), the same transition dipoles are used as for CIS

$$\mathbf{D}_{ij} = \langle\varphi_i|\hat{r}|\varphi_j\rangle \quad (12)$$

For the EOM-CC, the transition dipole matrix

$$\mathbf{D}_{ij} = \langle\varphi_0|\hat{L}_i \exp(-\hat{T})\hat{r} \exp(\hat{T})\hat{R}_j|\varphi_0\rangle \quad (13)$$

is not necessarily Hermitian. Adding a non-Hermitian component to the Hamiltonian can lead to complex eigenvalues, with the result that propagation of the wave function might no longer be norm-conserving. We approximate the EOM-CC transition dipole matrix by retaining only the Hermitian component $(\mathbf{D}_{ij} + \mathbf{D}_{ji}^*)/2$ and dropping the small, nonphysical, non-Hermitian component.

For the full solution of the TDSE, the sum in eq 9 extends over all bound states and the continuum. For practical applications, the sum needs to be restricted to a suitable subset of states. For example, CIS includes the ground state and only the singly excited states. CIS energies typically have errors of 1.0 eV[87] for valence excited states. Adding perturbative doubles corrections for electron correlation to the CIS excitation energies yields the

CIS(D) approach. This reduces the error to ca. 0.5 eV.[87] The equation-of-motion coupled-cluster singles and doubles (EOM-CCSD) method treats electron correlation in the ground and excited states using the coupled-clusters approach. The EOM-CCSD approach gives excitation energies that are within 0.3 eV[87,88] of the experimental results for valence excited states. Large multireference configuration interaction calculations would produce even more accurate excitation energies, but these are too costly for the size of molecules that we hope to study and for the number of states needed in the simulations. Within a given method [RPA, CIS, CIS(D), or EOM-CCSD], practical considerations limit the total number of states that can be used. Increasing the number of states included until no further change is seen in the simulation is one means of determining whether the number of states is adequate. Finite basis sets are usually used in molecular calculations. Because continuum functions are not included in the present calculations, the simulations cannot model ionization directly.

Table 1. Calculated Vertical Ionization Potentials for Butadiene[a]

	theory		
basis set	UHF	ROHF	UCCSD
6-31G(d,p)	7.561	7.929	8.790
6-31+G(d,p)	7.696	8.060	8.935
6-31++G(d,p)	7.694	8.058	8.934
6-31 2+ G(d,p)	7.697	8.061	8.943
6-31 3+ G(d,p)	7.697	8.061	8.943
6-311++G(2df,2pd)	7.700	8.091	9.151

[a] In eV; experimental value = 9.072 ± 0.007 eV.[91]

The present study uses a linearly polarized and spatially homogeneous external field

$$\mathbf{e}(\mathrm{r},t) \approx \mathbf{E}(t)\sin(\omega t + \varphi) \tag{14}$$

This is a good approximation for the laser field, because typical wavelengths are much larger than molecular dimensions. The simulations use a Gaussian envelope

$$g(t) = \exp[-\alpha(t/n\tau)^2] \tag{15}$$

$$\mathbf{E}(t) = \begin{cases} \mathbf{E}_{\max}[g(t - n\tau/2) - \Delta]/(1 - \Delta) & \text{for } 0 \le t \le n\tau \\ 0 & \text{for } t < 0 \text{ and } t > n\tau \end{cases} \tag{16}$$

where $\tau = 2\pi/\omega$ is the period and n is the number of cycles. The offset Δ is chosen so that $\mathbf{E}(0) = 0$ and $\mathbf{E}(n\tau) = 0$. For $\omega = 0.06$ au (760 nm) and $\alpha = 16 \ln 2$, $\Delta = 1/16$, $n \approx 3$, and the full width at half-maximum (fwhm) is ~4 fs (see Figure 5c below).

The RPA, CIS, CIS(D), and EOM-CCSD calculations were carried out with the development version of the Gaussian software package.[89] As in our previous studies,[82,83] *trans*-butadiene was optimized at the HF/6-31G(d,p) level of theory. Excited-state calculations were carried out with 6-31G(d,p), 6-31 n+ G(d,p), 6-31(n+)G(d,p), and 6-311++G(2df,2pd) basis sets. The 6-31 n+ G(d,p) basis has one set of five Cartesian d functions on the carbons, one set of p functions on hydrogen, and n sets of diffuse s and p functions on all carbons (n = 1, 2, and 3, with exponents of 0.04380, 0.01095, and 0.0027375, respectively). The modified 6-31(n+)G(d,p) basis set is derived from the 6-31 n+ G(d,p) basis set but has diffuse s and p functions only on the end carbons. A three-cycle Gaussian pulse with ω = 0.06 au (760 nm) was used in the simulations. For

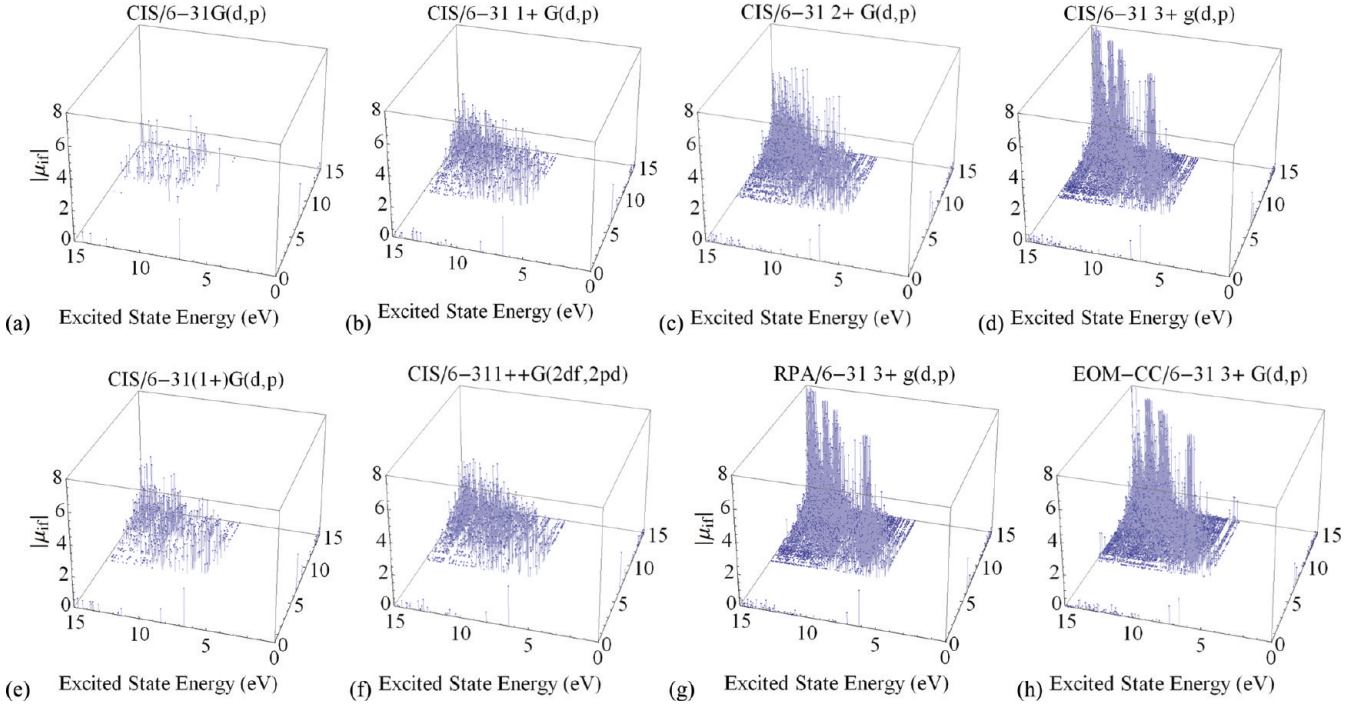

Figure 4. Transition dipoles for butadiene calculated with (a) CIS/6-31G(d,p), (b) CIS/6-31 1+ G(d,p), (c) CIS/6-31 2+ G(d,p), (d) CIS/6-31 3+ G(d,p), (e) CIS/6-31(1+)G(d,p), (f) CIS/6-31++G(2df,2pd), (g) RPA/6-31 3+ G(d,p), and (h) EOM-CC/6-31 3+ G(d,p).

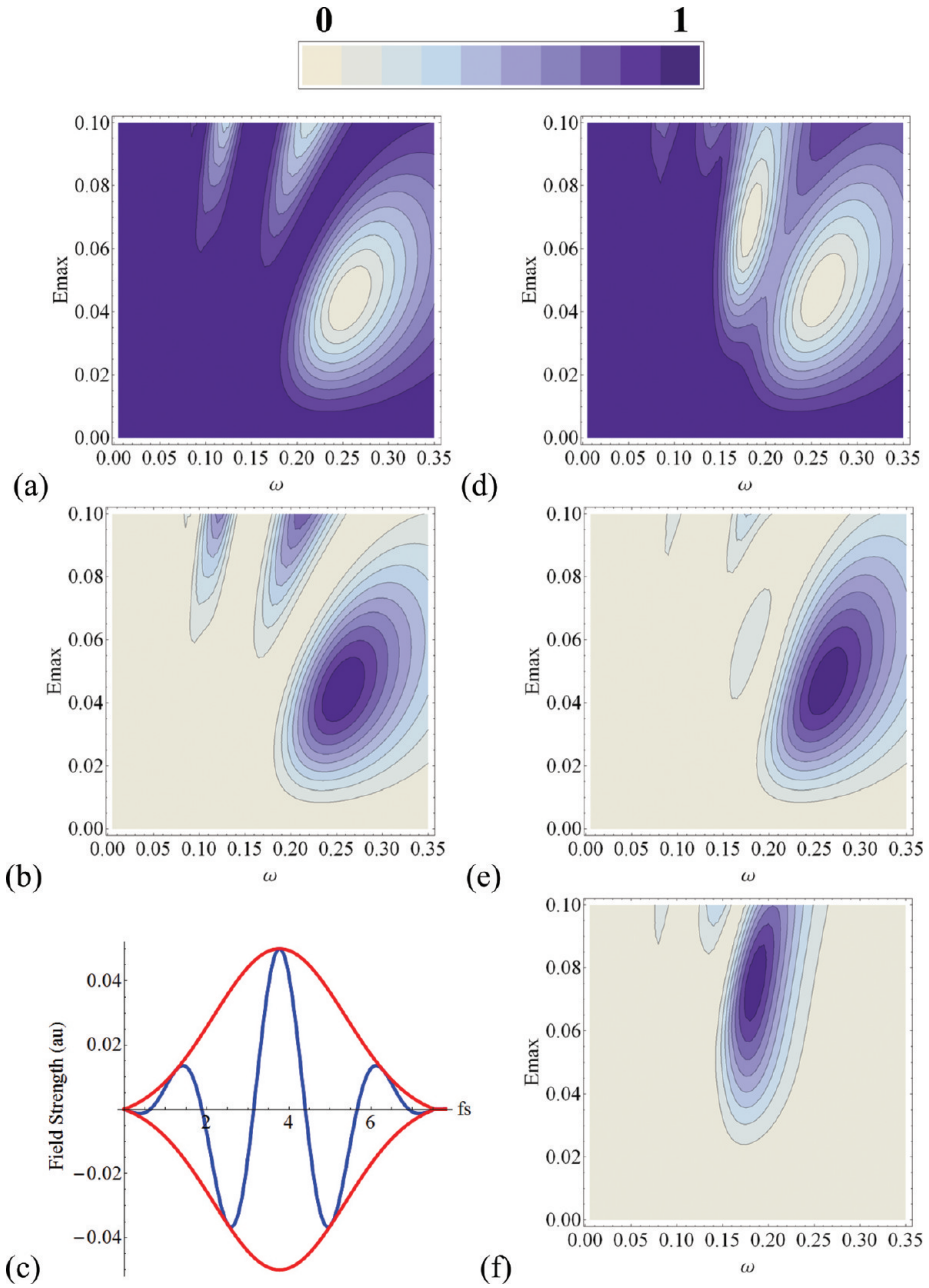

Figure 5. Response of model two- and three-level systems ($\omega_0 = 0$, $\omega_1 = 0.25$, $\omega_2 = 0.35$; $D_{01} = 2.0$, $D_{12} = 2.0$, $D_{02} = 0.0$ au) to a three-cycle Gaussian pulse, as a function of the pulse frequency, ω, and the maximum of the pulse envelope, E_{max}: (a,b) ground- and excited-state populations of the two-level system, (c) pulse shape, and (d−f) ground- and excited-state populations of the three-level system.

maximum effect, the field was directed along the long axis of the molecule, specifically along the vector connecting the end carbons. Up to 500 states were included in the simulations. Mathematica[90] was used to integrate the TD-CI equations and analyze the results. The TD-CI integrations were carried out with a step size of 0.5 au (0.012 fs). To facilitate plotting in Figures 8−10 below, the excited-state populations were represented by Gaussians with an energy width of 0.01 au fwhm.

RESULTS AND DISCUSSION

Orbitals and States. The ground-state Hartree−Fock (HF) wave function of *trans*-butadiene with C_{2h} symmetry consists of 13 σ orbitals (7 a_g and 6 b_u symmetry) and 2 π-bonding orbitals. With the 6-31G(d,p) basis set, the HOMO − 1 and HOMO (highest occupied molecular orbital) are π orbitals (π_1 and π_2, a_u and b_g symmetry, respectively), whereas the LUMO (lowest unoccupied molecular orbital) and LUMO + 1 are π^* orbitals (π_3 and π_4, a_u and b_g symmetry, respectively), as shown in Figure 1. The states involving these four π states have large transition dipole moments that play an important role in the response of butadiene to intense laser pulses. The ground-state wave function is ^1A_g. The RPA, CIS, CIS(D), and EOM-CC levels of theory concur that the lowest singlet excited state is ^1B_u and corresponds to the HOMO → LUMO ($\pi_2 \rightarrow \pi_3$, $1b_g \rightarrow 2a_u$) excitation. Three additional low-lying singlet states can be

dx.doi.org/10.1021/jp107384p |J. Phys. Chem. A 2011, 115, 4678–4690

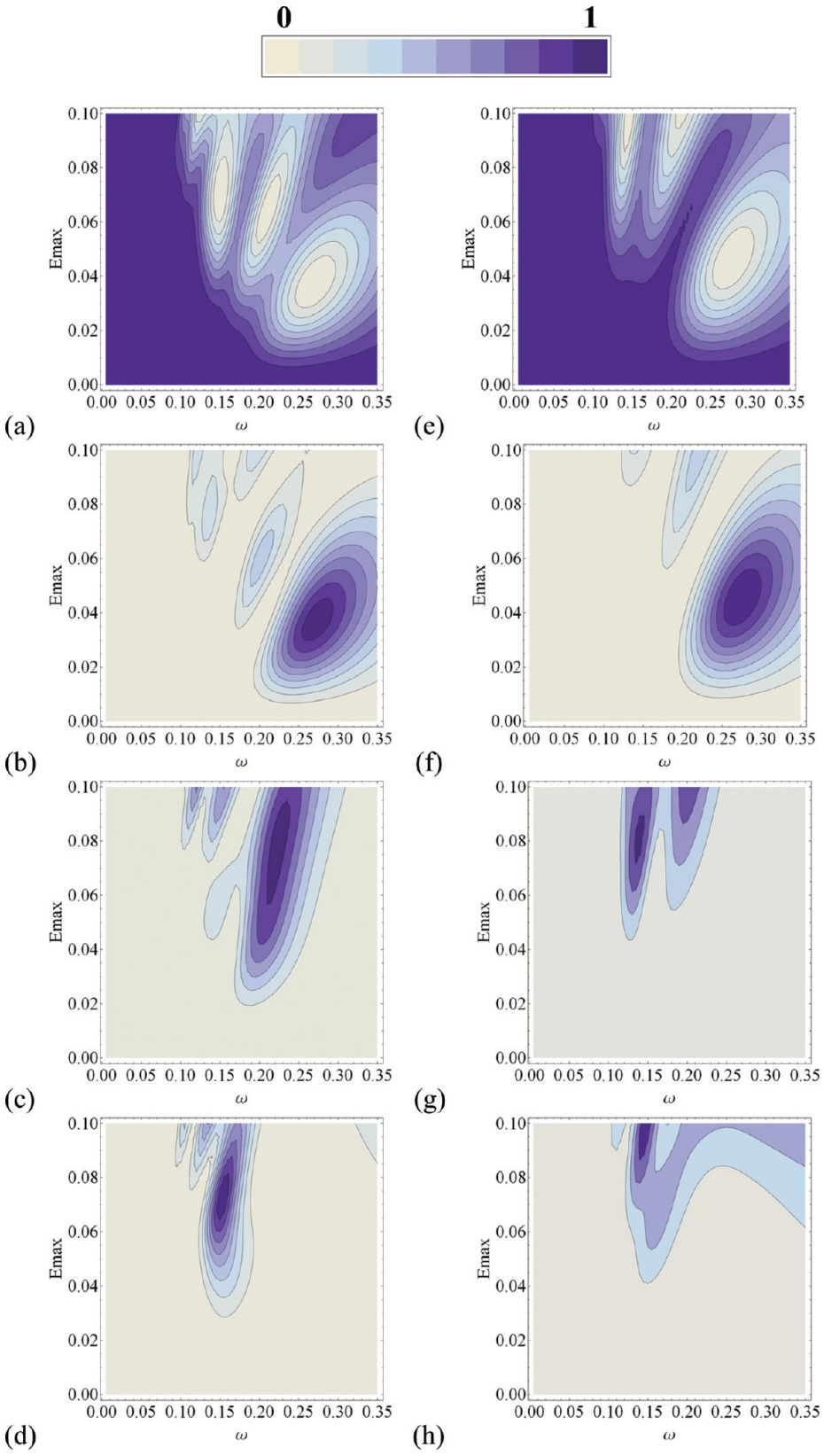

Figure 6. Response of the butadiene π states ($1\ ^1A_g$ ground state and the $1\ ^1B_u$, $2\ ^1A_g$, and $2\ ^1B_u$ excited states) to a three-cycle Gaussian pulse: (a−d) CIS/6-31G(d,p) excited-state energies and transition dipoles: $\omega_0 = 0.0$, $\omega_1 = 0.256$, $\omega_2 = 0.344$, $\omega_3 = 0.369$, $\omega_4 = 0.460$; $D_{02} = D_{03} = D_{14} = D_{23} = 0.0$, $D_{01} = -2.575$, $D_{04} = 0.485$, $D_{12} = 0.430$, $D_{13} = 2.620$, $D_{24} = 0.547$, $D_{34} = 3.406$ au. (e−h) EOM-CC/6-31G(d,p) excited-state energies and transition dipoles: $\omega_0 = 0.0$, $\omega_1 = 0.267$, $\omega_2 = 0.293$, $\omega_3 = 0.358$, $\omega_4 = 0.440$; $D_{02} = D_{03} = D_{14} = D_{23} = 0.0$, $D_{01} = -2.091$, $D_{04} = 0.555$, $D_{12} = -1.581$, $D_{13} = -0.330$, $D_{24} = -1.968$, $D_{34} = -0.114$ au.

dx.doi.org/10.1021/jp107384p |*J. Phys. Chem. A* 2011, 115, 4678–4690

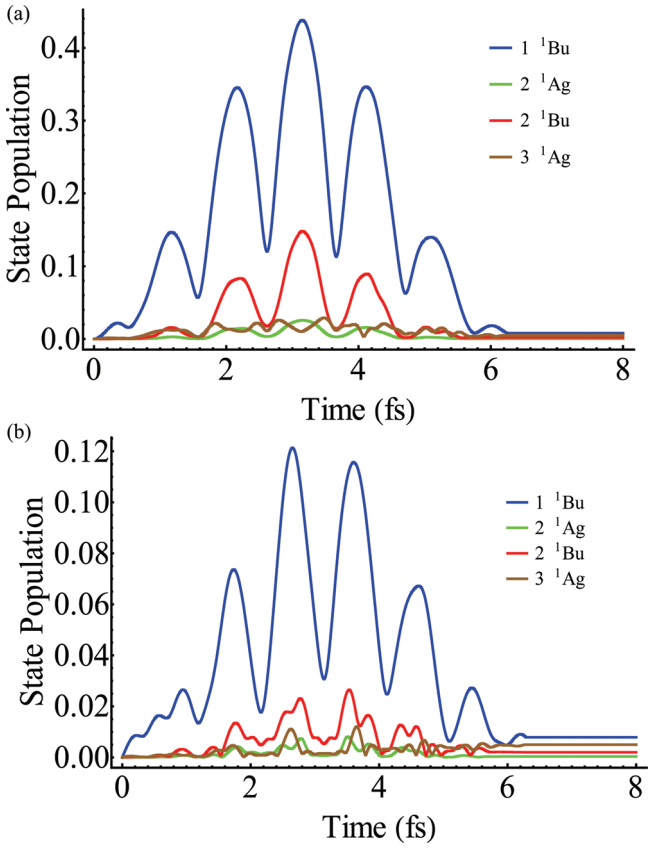

Figure 7. Comparison of the response of butadiene calculated with TD-CIS/6-31G(d,p) in a three-cycle Gaussian pulse (ω = 0.06 au, E_{max} = 0.05 au) in terms of (a) the zero-field states and (b) the instantaneous adiabatic states.

constructed from the π orbitals: the in-phase and out-of-phase linear combinations of the $\pi_2 \rightarrow \pi_4$ and $\pi_1 \rightarrow \pi_3$ excitations ($\pi_2 \rightarrow \pi_4 \pm \pi_1 \rightarrow \pi_3$) ($^1A_g$ symmetry) and $\pi_1 \rightarrow \pi_4$ (^1B_u symmetry). The doubly excited configuration that excites two electrons from the HOMO to the LUMO, $2 \times \pi_2 \rightarrow \pi_3$, is also ^1A_g symmetry and mixes strongly with the $\pi_2 \rightarrow \pi_4 + \pi_1 \rightarrow \pi_3$ configuration. Because EOM-CC calculations include doubly excited configurations, this excited state is calculated to be considerably lower in energy by EOM-CC than by RPA and CIS.

As the basis set size is increased from 6-31G(d,p) to 6-31 3+ G(d,p), numerous low-lying unoccupied diffuse, Rydberg-like orbitals start to appear between the smaller basis set HOMO and LUMO orbitals, complicating the qualitative description of the electronic states. The energies of the first 30 excited states of ^1A_g and ^1B_u symmetry calculated by RPA, CIS, CIS(D), and EOM-CC with the 6-31 3+ G(d,p) basis set are compared in Figure 2. (Because of the symmetry of the transition dipoles, states with A_u and B_g symmetry are not coupled to the A_g and B_u states by the in-plane electric field used in the simulations discussed below.) Except for the lowest ^1B_u state, the $\pi \rightarrow \pi^*$ states are embedded in a sea of Rydberg-like and pseudocontinuum states arising from diffuse, low-energy unoccupied orbitals. Beyond the first few states, the EOM-CC excitation energies are significantly lower than the CIS and RPA excitation energies because of the admixture of higher excitations. CIS(D) captures most of this energy lowering compared to EOM-CC, but perturbation theory can overestimate or underestimate the correction arising from double excitations. Because this becomes more problematic for higher-energy states (see Figure 3a), the perturbative corrections for states above 11 eV are limited so that $0.8E_i^{CIS} \leq E_i^{CIS(D)} \leq E_i^{CIS}$ (this affects ca. 10−20 states out of 500 for each of the various basis sets). As shown in the inset in Figure 3b, adding more diffuse functions increases the number of states below the ionization threshold. In the pseudocontinuum above the ionization potential (IP), the excited-state energies increase approximately linearly with the number of states (see Figure 3b). The density of states, given by the inverse of the slope of the lines, increases roughly in proportion to the number of diffuse functions added, but also depends on the location and exponents of the diffuse functions.

The vertical ionization potentials (IPs) of butadiene, calculated with the unrestricted and restricted open-shell Hartree−Fock (UHF and ROHF, respectively) and coupled-cluster methods using various basis sets, are listed in Table 1. The ROHF and UHF IPs are ca. 1 and 1.4 eV lower than the experimental value, 9.072 ± 0.007 eV.[91] The CCSD calculations are within 0.15 eV of the experimental value provided that diffuse functions are included in the basis set. Figure 2 indicates that only a few of the calculated excited states of ^1A_g and ^1B_u symmetry are below the IP.

Transition Dipoles. The transition dipoles are summarized graphically in Figure 4 for states up to 15 eV. For each transition, the horizontal coordinates indicate the energies of the two states, and the height of the line is given by the magnitude of the transition dipole. The ground-to-excited-state transitions are along the two edges of the plot, whereas the excited-to-excited-state transitions are in the interior. The first ionization threshold is ca. 9 eV, and the dense forest of lines above this energy is the result of transitions between pseudocontinuum states. The lines are peaked near the diagonal, as would be expected from continuum states. The effect of basis set size can be seen in Figure 4a−f. The forest of lines is far too sparse with the 6-31G(d,p) basis set but is much denser for the larger basis sets. The densities of the lines look similar with the 6-31(1+)G(d,p), 6-31 1+ G(d,p), and 6-311++G(2df,2pd) basis sets (Figure 4b, e,f). The 6-31 n+ G(d,p) results (Figure 4b−d) become progressively denser and more strongly peaked along the diagonal, indicating a better representation of the pseudocontinuum states. Because multiple diffuse functions (Figure 4c,d) appear to be more important than higher polarization functions (Figure 4f) for representing the states in the pseudocontinuum, the RPA, CIS, CIS(D), and EOM-CC calculations are compared using the 6-31 3+ G(d,p) basis set rather than the 6-311++G(2df,2pd) basis set. Parts d, g, and h of Figure 4 show that the CIS, RPA, and EOM-CC transition dipoles with the 6-31 3+ G(d,p) basis set are very similar on the scale of these plots. Because the CIS(D) perturbative corrections are applied to the energies but not the transition dipoles, the CIS(D) figure (not shown) closely resembles the CIS results. Because the EOM-CC calculations include double excitations, some of the transition dipoles between valence states are smaller (particularly the lowest ^1B_u-to-^1A_g $\pi \rightarrow \pi^*$ transitions). However, the transition dipoles between the pseudocontinuum states are similar in appearance to the RPA and CIS results.

Simulations with Model Systems. Because the transitions from the ground state to the ^1B_u states are the most intense absorptions and these transitions involve the π orbitals, early work on polyenes in strong fields modeled the response by considering only the π orbitals.[55,56] To help understand the response of butadiene, we first examined the behavior of some simple models of the π states. Figure 5 shows the results of

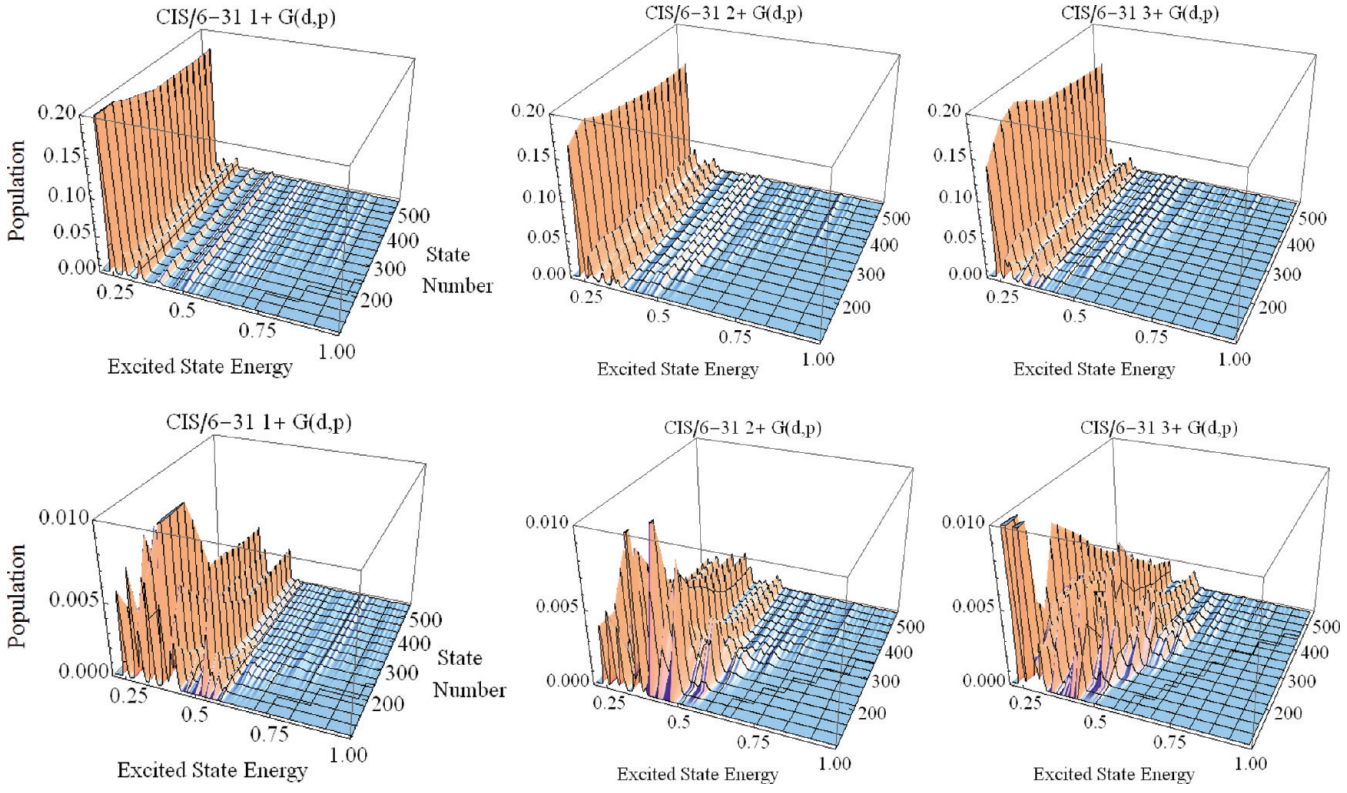

Figure 8. Excited-state populations of butadiene as a function of number of states included in the TD-CIS simulation, at the maximum of the pulse (top row) and after the pulse (bottom row) (ω = 0.06 au, E_{max} = 0.05 au) with the 6-31 n+ G(d,p) basis sets.

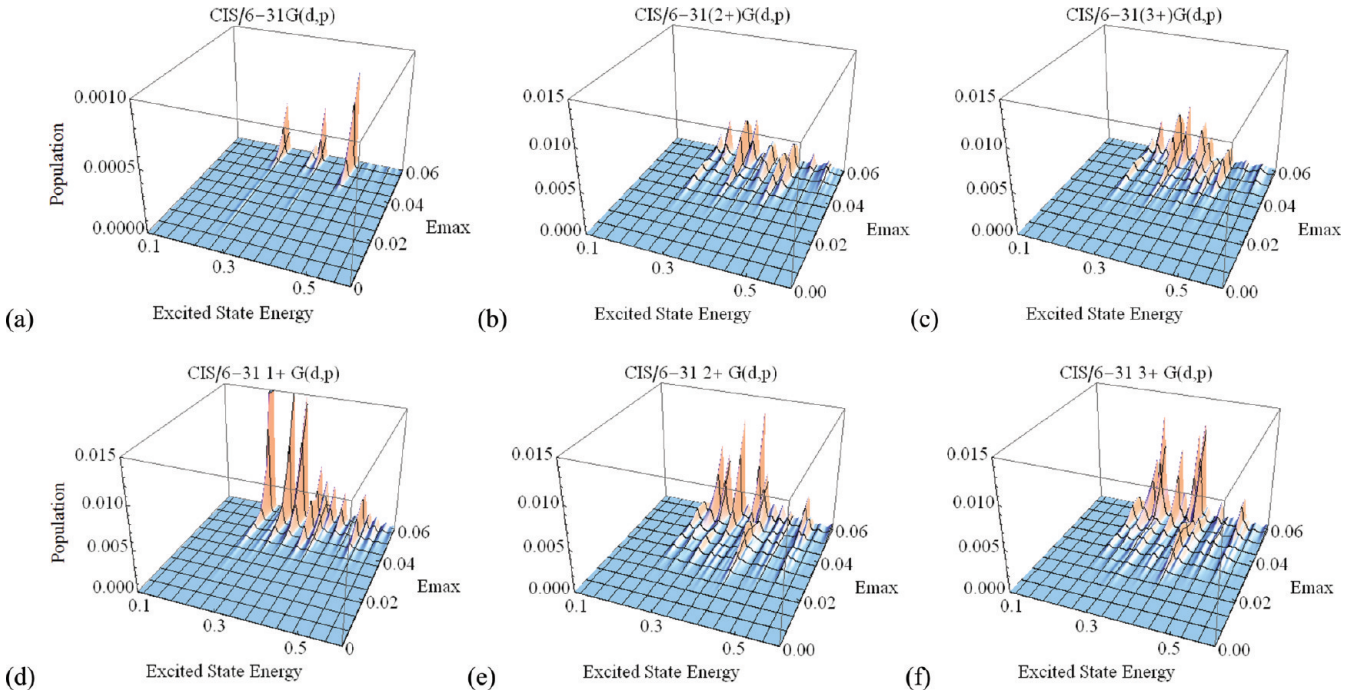

Figure 9. Response of butadiene subjected to a three-cycle Gaussian pulse (ω = 0.06 au, E_{max} = 0−0.06 au) calculated by TD-CIS with 500 excited states using the following basis sets: (a) 6-31G(d,p), (b) 6-31(2+)G(d,p), (c) 6-31(3+)G(d,p), (d) 6-31 1+ G(d,p), (e) 6-31 2+ G(d,p), and (f) 6-31 3+ G(d,p).

TD-CI simulations with model two- and three-level systems, as well as the shape of a three-cycle Gaussian pulse used in the simulations. The energies and transition dipoles for the model systems were chosen to be comparable to the lowest $\pi \rightarrow \pi^*$ excitation energies and transition dipoles of butadiene calculated with CIS/6-31G(d,p) (ω_0 = 0, ω_1 = 0.25, ω_2 = 0.35; D_{01} = 2.0, D_{12} = 2.0,

dx.doi.org/10.1021/jp107384p |J. Phys. Chem. A 2011, 115, 4678–4690

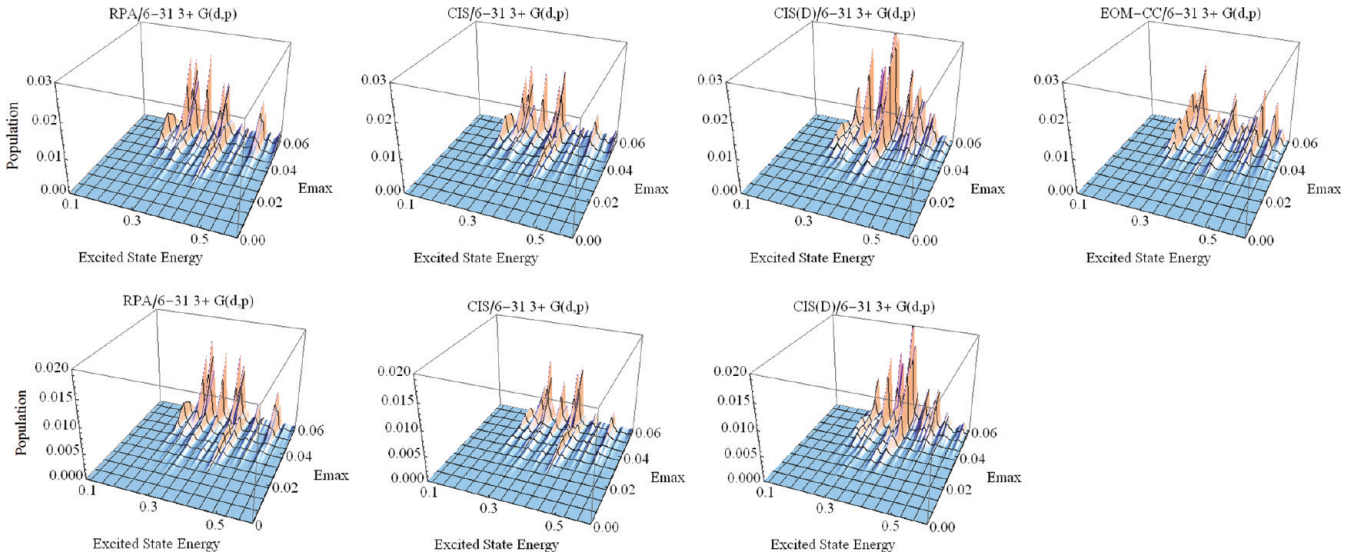

Figure 10. Response of butadiene subjected to a three-cycle Gaussian pulse (ω = 0.06 au, E_{max} = 0−0.06 au) calculated with the 6-31 3+ G(d,p) basis set and RPA, CIS, CIS(D), and EOM-CC using 300 states (top row) and 500 states (bottom row).

D_{02} = 0.0 au). The maximum of the Gaussian pulse envelope was varied from 0 to 0.1 au (vertical axis), and the frequency of the pulse ranged from 0.01 to 0.35 au (horizontal axis). The populations for the ground and excited states of the two-level system are shown in Figure 5a,b. The prominent peak indicates that population inversion is achieved for $E_{max} \approx 0.044$ au when the frequency is slightly higher than the one-photon resonance, ω = 0.25 au. This corresponds to a π pulse, and the displacement to higher energy is due to Stark shifting. The other peaks are the result of higher-order processes. The populations for the three-level system are shown in Figure 5d−f. The behavior of the first excited state as a function of E_{max} and ω is similar to that of the two-level model (Figure 5e vs 5b). The peak in the population of the second excited state (Figure 5f) corresponds to a two-photon process (this was verified by changing the energy of the second excited state).

Simulations with Butadiene. Figure 6 illustrates the results of simulations for a simple model of butadiene using only the ground state and the four lowest π states computed by TD-CIS and TD-EOMCC with the 6-31G(d,p) basis set. The responses of the ^1A_g ground state and the lowest ^1A_g excited state and the lowest two ^1B_u excited states are shown; the population of the second ^1A_g excited state remains less than 0.1 for the range of E_{max} and ω values examined because the transition dipoles with the other π states are small. The ground state is coupled to the lowest ^1B_u state with a large transition dipole. Likewise, large transition dipoles couple this ^1B_u state to the ^1A_g state and the ^1A_g state to the higher ^1B_u state. This can be compared to the two- and three-level systems shown in Figure 5. As expected, the response of the first excited state in butadiene is very similar to that of the first excited state in the two- and three-level systems, dominated by the peak for the one-photon process. The peak in the population of the lowest ^1A_g excited state corresponds to a two-photon process, and the peak shown for the second ^1B_u state corresponds to a three-photon process (as confirmed by dependence of the peak position on the energy of the states; the one-photon transition from the ^1A_g ground state to the ^1A_g excited state is dipole-forbidden). Because of the significant contribution of two-electron excitations to the ^1A_g π excited state in the EOM-CC calculations, the transition dipoles coupling this state to the ^1B_u states are about 40% smaller than in the CIS calculations. As a result, the responses of both the ^1A_g state and the second ^1B_u excited state are much weaker in the TD-EOMCC simulation. The regions of decrease in the population of the ground state correspond to the peaks in the population of the excited states because the populations must sum to unity. Inspection of Figure 6 shows that the conditions used for subsequent simulations (ω = 0.06, E_{max} up to 0.06 au) are well away from any single- or multiphoton resonances.

The populations of the four lowest π states during a three-cycle Gaussian pulse are shown in Figure 7. In terms of both the zero-field states and the instantaneous adiabatic states (defined as the fully relaxed states in the instantaneous electric field), the populations change rapidly as the molecule is polarized by the electric field of the pulse, with the largest response coming from the lowest ^1B_u state and the next largest from the lowest ^1A_g excited state (which is strongly coupled to the lowest ^1B_u state). The changes in the populations of the instantaneous adiabatic states are less than half the size of those seen for zero-field states, but they are still much larger than the final populations after the pulse. Because these fluctuations are so large, it is not readily possible to track the details of the excitation from state to state during the pulse by using the instantaneous adiabatic states. However, the results of the interaction can still be assessed by examining the populations after the pulse.

The calculated response of butadiene to a short, intense pulse depends on the number of excited states included in the simulation as well as the theory and basis set used for the excited-state calculations. An estimate of the number of excited states needed can be obtained by comparing the static polarizability computed with the sum-over-states formalism to the one calculated by linear-response theory. Using the RPA data with the 6-31 n+ G(d,p) basis sets, approximately 120, 210, 340, and 460 states are required for n = 0−3, respectively, to converge the longitudinal polarizability to within 3% of the linear-response value. The dependence of the simulations on the number of states is shown in Figure 8 for a three-cycle Gaussian pulse with ω = 0.06 au and E_{max} = 0.05 au and calculated with TD-CIS/6-31 n+ G(d,p),

$n = 1-3$. The top row of Figure 8 shows that, at the maximum of the pulse, the populations do not depend strongly on the number of states. The largest response is for the 1 ^1B_u excited state, and the contribution is similar in magnitude for these basis sets. For the 2+ and 3+ basis sets, the 2 ^1B_u and 3 ^1B_u states are low in energy and show a significant response as well. The larger basis sets also have many more low-lying Rydberg-like and pseudo-continuum states. Even though their response is small, the sum of their contributions is significant and more states are needed in the sum over states calculation of the polarizability and in the TD-CI simulations in order to properly represent the interaction with the field. The populations after the pulse are much smaller but are more sensitive to the quality of the simulation because they depend on the cumulative response over the entire pulse. The bottom row of Figure 8 shows the results after the pulse and indicates that 250, 400, and ca. 500 states are needed with the 6-31 n+ G(d,p) basis sets for $n = 1-3$, respectively. This again illustrates that the small contributions from the numerous low-lying pseudocontinuum states are important for stable simulations under these conditions. Similar results were found for simulations with other levels of theory.

Figures 9 and 10 summarize the effect of basis sets and levels of theory on the response of butadiene to a three-cycle Gaussian pulse ($\omega = 0.06$ au). Populations are plotted as a function of the excited-state energies and field strengths up to E_{max} =0.06 au (1.26×10^{14} W cm^{-2}). Figure 9 collects the results of TD-CIS simulations using 500 states and employing excitation energies and transition dipoles calculated with various basis sets. As expected, the populations of the excited states increase dramatically with the field strength. Above a threshold in the maximum field strength, many excited states are populated, signaling an increase in the ionization rate. Details of the populations in specific states are very sensitive to the level of theory, basis set, and number of states used in the simulation. Nevertheless, some general trends can be discerned. Without diffuse functions, the response is too weak (Figure 9a, note the 15-fold difference in the vertical scale). Adding 2 and 3 sets of diffuse functions on the end carbons (Figure 9b,c) increases the response, but not as much as putting one set of diffuse functions on each carbon (Figure 9d). With two sets of diffuse functions (Figure 9e), significant excitation already occurs at lower field strengths. Augmenting the 6-31 2+ G(d,p) basis with a set of sp diffuse functions on the hydrogens increases the response somewhat more (not shown). The results with 3 sets of diffuse functions are very similar to 2 sets (Figure 9f vs 9e). Similar trends in basis set effects are found for RPA and CIS(D) simulations with 500 states.

The top row of Figure 10 compares TD-CI simulations with 300 states based on RPA, CIS, CIS(D), and EOM-CC calculations with the 6-31 3+ G(d,p) basis set. The RPA and CIS results are very similar, while the CIS(D) response is somewhat stronger at higher E_{max}. The EOM-CC response is comparable to or slightly less than CIS and RPA. The results of simulations with RPA, CIS, and CIS(D) using 500 states are shown in the bottom row of Figure 10. [EOM-CC/6-31 3+ G(d,p) calculations with 500 states are not practical at this time.] With the 6-31 3+ G(d,p) basis, the 500-state simulations follow the same trend as with 300 states. However, with small basis sets such as 6-31G(d,p) (not shown), the differences between the various levels of theory are more pronounced.

Because the populations of individual excited states are very sensitive to the level of theory, it is useful to compare some aggregate quantities. The depletion of the population of the ground state is equal to the sum of the excited-state populations generated by the interaction with the intense pulse. Figure 11a shows the population of the ground state as a function of field strength for simulations with 300 states for various levels of theory and the 6-31 3+ G(d,p) basis set. Up to a maximum field strength of ca. 0.035 au, the RPA, CIS, CIS(D), and EOM-CC ground-state populations are nearly identical and show less than a 2% depletion. For E_{max} greater than ca. 0.035 au, there is a rapid decrease in the ground-state contribution as excited states become more populated. In agreement with Figure 10, the responses of RPA, CIS and EOM-CC are similar but CIS(D) is significantly stronger. Similar trends were found for simulations

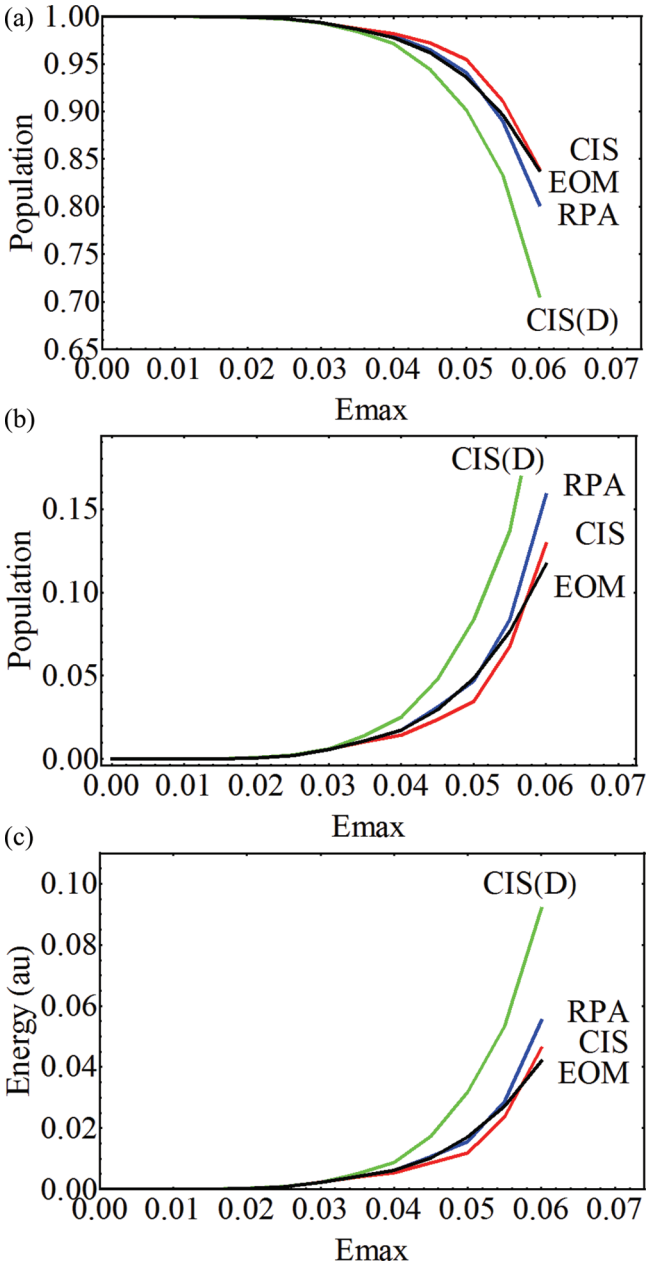

Figure 11. Dependence of the populations and energies on E_{max}, the maximum field strength of the pulse: (a) ground-state population, (b) sum of the populations of excited states with energies less than 0.5 au, (c) energy deposited in excited states with energies less than 0.5 au [RPA, blue; CIS, red; CIS(D), green; EOM-CC, black].

dx.doi.org/10.1021/jp107384p |J. Phys. Chem. A 2011, 115, 4678–4690

with 500 states (not shown). Figure 11b compares the sum of the populations of the excited states with energies less than 0.5 au. The results are in accord with Figure 10, as well as with the trends the ground-state populations (Figure 11a). Interaction with the intense pulse deposits energy into the molecule by populating excited states. Figure 11c compares the sum of the excited-state energies weighted by their populations for excited states with energies less than 0.5 au. Again, the values for RPA, CIS, and EOM-CC are similar but CIS(D) is significantly larger. For simulations with 500 states, the amount of energy deposited in this range of states is smaller, but the trends are similar.

SUMMARY

The lowest singlet excited state of butadiene is a ^1B_u $\pi \rightarrow \pi^*$ state and is treated fairly well by RPA, CIS, and CIS(D) when compared to EOM-CC. CIS(D) reproduces the trends in energy of the higher bound and pseudocontinuum states better than by RPA and CIS when compared to EOM-CC, but the perturbative correction for doubles can be erratic. The effect of the basis set can be seen rather dramatically by looking at the dipole moments for transitions between ground and excited states and between excited states. Diffuse functions are particularly important for transitions between excited states in the pseudocontinuum, above the first ionization threshold. Higher polarization functions seem to be less important, whereas multiple diffuse functions should be placed on all of the heavy atoms and not just on the end carbons. Transition dipoles involving the low-lying π states are smaller for EOM-CC than for CIS and RPA because the latter do not take into account the double excitation character of some of these states. Studies with two- and three-level model systems as well as models involving only the low-lying π states of butadiene show that intense three-cycle pulses can cause resonant two- and three-photon transitions. The frequency and intensity ranges for the pulse used in the simulations were chosen to avoid these resonances. Nevertheless, above a threshold in intensity of the pulse, there is rapid population of higher states in the pseudocontinuum. The response depends on the level of theory, the basis set, and the number of excited states used in the simulation. Depending on the basis set, 500 excited states or more might be needed. For the pulse parameters selected, the response is far too weak with small basis sets such as 6-31G(d,p), but consistent results are achieved with two and three sets of sp diffuse functions on each carbon. For small basis sets, the difference between levels of theory is more pronounced, but with two and three sets of diffuse functions, the CIS, RPA, and EOM-CC results are similar, whereas the CIS(D) response is too strong when compared to the more reliable EOM-CC calculations.

AUTHOR INFORMATION

Corresponding Author

*E-mail: hbs@chem.wayne.edu.

ACKNOWLEDGMENT

This work was supported by a grant from the National Science Foundation (CHE0910858). Wayne State University's computing grid and the NCSA Teragrid provided computational support. We also thank Stanley M. Smith for helpful discussions and acknowledge an ongoing collaboration with Robert J. Levis at Temple University in the area of strong-field chemistry that provided the stimulus for the present study. J.A.S. thanks the IMSD Program at WSU for financial support (GM058905-11).

REFERENCES

(1) Baltuska, A.; Udem, T.; Uiberacker, M.; Hentschel, M.; Goulielmakis, E.; Gohle, C.; Holzwarth, R.; Yakoviev, V. S.; Scrinzi, A.; Hansch, T. W.; Krausz, F. Attosecond control of electronic processes by intense light fields. *Nature* **2003**, *421*, 611.

(2) Brabec, T.; Krausz, F. Intense few-cycle laser fields: Frontiers of nonlinear optics. *Rev. Mod. Phys.* **2000**, *72*, 545.

(3) Cavalieri, A. L.; Muller, N.; Uphues, T.; Yakovlev, V. S.; Baltuska, A.; Horvath, B.; Schmidt, B.; Blumel, L.; Holzwarth, R.; Hendel, S.; Drescher, M.; Kleineberg, U.; Echenique, P. M.; Kienberger, R.; Krausz, F.; Heinzmann, U. Attosecond spectroscopy in condensed matter. *Nature* **2007**, *449*, 1029.

(4) Corkum, P. B.; Krausz, F. Attosecond science. *Nat. Phys.* **2007**, *3*, 381.

(5) Goulielmakis, E.; Schultze, M.; Hofstetter, M.; Yakovlev, V. S.; Gagnon, J.; Uiberacker, M.; Aquila, A. L.; Gullikson, E. M.; Attwood, D. T.; Kienberger, R.; Krausz, F.; Kleineberg, U. Single-cycle nonlinear optics. *Science* **2008**, *320*, 1614.

(6) Goulielmakis, E.; Yakovlev, V. S.; Cavalieri, A. L.; Uiberacker, M.; Pervak, V.; Apolonski, A.; Kienberger, R.; Kleineberg, U.; Krausz, F. Attosecond control and measurement: Lightwave electronics. *Science* **2007**, *317*, 769.

(7) Ivanov, M. Y.; Spanner, M.; Smirnova, O. Anatomy of strong field ionization. *J. Mod. Opt.* **2005**, *52*, 165.

(8) Kling, M.; Krausz, F. Attoscience: An attosecond stopwatch. *Nat. Phys.* **2008**, *4*, 515.

(9) Kling, M. F.; Vrakking, M. J. J. Attosecond electron dynamics. *Annu. Rev. Phys. Chem.* **2008**, *59*, 463.

(10) Uiberacker, M.; Uphues, T.; Schultze, M.; Verhoef, A. J.; Yakovlev, V.; Kling, M. F.; Rauschenberger, J.; Kabachnik, N. M.; Schroder, H.; Lezius, M.; Kompa, K. L.; Muller, H. G.; Vrakking, M. J. J.; Hendel, S.; Kleineberg, U.; Heinzmann, U.; Drescher, M.; Krausz, F. Attosecond real-time observation of electron tunnelling in atoms. *Nature* **2007**, *446*, 627.

(11) Drescher, M.; Hentschel, M.; Kienberger, R.; Tempea, G.; Spielmann, C.; Reider, G. A.; Corkum, P. B.; Krausz, F. X-ray pulses approaching the attosecond frontier. *Science* **2001**, *291*, 1923.

(12) Krausz, F.; Ivanov, M. Attosecond physics. *Rev. Mod. Phys.* **2009**, *81*, 163.

(13) Akagi, H.; Otobe, T.; Staudte, A.; Shiner, A.; Turner, F.; Dorner, R.; Villeneuve, D. M.; Corkum, P. B. Laser Tunnel Ionization from Multiple Orbitals in HCl. *Science* **2009**, *325*, 1364.

(14) Smirnova, O.; Mairesse, Y.; Patchkovskii, S.; Dudovich, N.; Villeneuve, D.; Corkum, P.; Ivanov, M. Y. High harmonic interferometry of multi-electron dynamics in molecules. *Nature* **2009**, *460*, 972.

(15) Worner, H. J.; Bertrand, J. B.; Kartashov, D. V.; Corkum, P. B.; Villeneuve, D. M. Following a chemical reaction using high-harmonic interferometry. *Nature* **2010**, *466*, 604.

(16) Sussman, B. J.; Townsend, D.; Ivanov, M. Y.; Stolow, A. Dynamic stark control of photochemical processes. *Science* **2006**, *314*, 278.

(17) Itatani, J.; Levesque, J.; Zeidler, D.; Niikura, H.; Pepin, H.; Kieffer, J. C.; Corkum, P. B.; Villeneuve, D. M. Tomographic imaging of molecular orbitals. *Nature* **2004**, *432*, 867.

(18) Gessner, O.; Lee, A. M. D.; Shaffer, J. P.; Reisler, H.; Levchenko, S. V.; Krylov, A. I.; Underwood, J. G.; Shi, H.; East, A. L. L.; Wardlaw, D. M.; Chrysostom, E. T.; Hayden, C. C.; Stolow, A. Femtosecond multidimensional imaging of a molecular dissociation. *Science* **2006**, *311*, 219.

(19) Haessler, S.; Caillat, J.; Boutu, W.; Giovanetti-Teixeira, C.; Ruchon, T.; Auguste, T.; Diveki, Z.; Breger, P.; Maquet, A.; Carre, B.; Taieb, R.; Salieres, P. Attosecond imaging of molecular electronic wavepackets. *Nat. Phys.* **2010**, *6*, 200.

(20) Kienberger, R.; Hentschel, M.; Uiberacker, M.; Spielmann, C.; Kitzler, M.; Scrinzi, A.; Wieland, M.; Westerwalbesloh, T.; Kleineberg, U.; Heinzmann, U.; Drescher, M.; Krausz, F. Steering attosecond electron wave packets with light. *Science* **2002**, *297*, 1144.

(21) Meckel, M.; Comtois, D.; Zeidler, D.; Staudte, A.; Pavicic, D.; Bandulet, H. C.; Pepin, H.; Kieffer, J. C.; Dorner, R.; Villeneuve, D. M.; Corkum, P. B. Laser-induced electron tunneling and diffraction. *Science* **2008**, *320*, 1478.

(22) Niikura, H.; Legare, F.; Hasbani, R.; Bandrauk, A. D.; Ivanov, M. Y.; Villeneuve, D. M.; Corkum, P. B. Sub-laser-cycle electron pulses for probing molecular dynamics. *Nature* **2002**, *417*, 917.

(23) Shafir, D.; Mairesse, Y.; Villeneuve, D. M.; Corkum, P. B.; Dudovich, N. Atomic wavefunctions probed through strong-field light-matter interaction. *Nat. Phys.* **2009**, *5*, 412.

(24) Stolow, A.; Underwood, J. G. Time-Resolved Photoelectron Spectroscopy of Nonadiabatic Dynamics in Polyatomics Molecules. *Adv. Chem. Phys.* **2008**, *139*, 497.

(25) Chelkowski, S.; Zuo, T.; Bandrauk, A. D. Ionization Rates of H_2^+ in an Intense Laser Field by Numerical Integration of the Time-Dependent Schrödinger Equation. *Phys. Rev. A* **1992**, *46*, R5342.

(26) Zuo, T.; Bandrauk, A. D. Superdressed H_2^+ and H_3^{2+} Molecular Ions in Intense, High-Frequency Laser Fields. *Phys. Rev. A* **1995**, *51*, R26.

(27) Chelkowski, S.; Zuo, T.; Atabek, O.; Bandrauk, A. D. Dissociation, Ionization, and Coulomb Explosion of H_2^+ in an Intense Laser Field by Numerical Integration of the Time-Dependent Schrödinger Equation. *Phys. Rev. A* **1995**, *52*, 2977.

(28) Yu, H. T.; Zuo, T.; Bandrauk, A. D. Molecules in intense laser fields: Enhanced ionization in a one-dimensional model of H_2. *Phys. Rev. A* **1996**, *54*, 3290.

(29) Chelkowski, S.; Foisy, C.; Bandrauk, A. D. Electron−nuclear dynamics of multiphoton H_2^+ dissociative ionization in intense laser fields. *Phys. Rev. A* **1998**, *57*, 1176.

(30) Walsh, T. D. G.; Ilkov, F. A.; Chin, S. L.; Chateauneuf, F.; Nguyen-Dang, T. T.; Chelkowski, S.; Bandrauk, A. D.; Atabek, O. Laser-induced processes during the Coulomb explosion of H_2 in a Ti-sapphire laser pulse. *Phys. Rev. A* **1998**, *58*, 3922.

(31) Bandrauk, A. D.; Lu, H. Z. Enhanced ionization of the molecular ion H_2^+ in intense laser and static magnetic fields. *Phys. Rev. A* **2000**, *62*, 53406.

(32) Bandrauk, A. D.; Chelkowski, S.; Zamojski, M. Laser phase control of electron−nuclear dynamics in dissociative ionization with intense femtosecond pulses: Exact (non-Born−Oppenheimer) numerical simulations for H_2^+. *Z. Phys. Chem.* **2000**, *214*, 1393.

(33) Talebpour, A.; Vijayalakshmi, K.; Bandrauk, A. D.; Nguyen-Dang, T. T.; Chin, S. L. Dissociative ionization of D_2 in intense laser fields: D^+-ion production perpendicular to the polarization of a 400-nm laser field. *Phys. Rev. A* **2000**, *62*, 42708.

(34) Kawata, I.; Kono, H.; Fujimura, Y.; Bandrauk, A. D. Intense-laser-field-enhanced ionization of two-electron molecules: Role of ionic states as doorway states. *Phys. Rev. A* **2000**, *62*, 31401.

(35) Bandrauk, A. D.; Chelkowski, S. Asymmetric electron−nuclear dynamics in two-color laser fields: Laser phase directional control of photofragments in H_2^+. *Phys. Rev. Lett.* **2000**, *84*, 3562.

(36) Kawata, I.; Bandrauk, A. D.; Kono, H.; Fujimura, Y. Enhanced ionization of the two-electron molecule H_2 in intense laser fields: Mechanism of the creation of doorway states. *Laser Phys.* **2001**, *11*, 188.

(37) Harumiya, K.; Kono, H.; Fujimura, Y.; Kawata, I.; Bandrauk, A. D. Intense laser-field ionization of H_2 enhanced by two-electron dynamics. *Phys. Rev. A* **2002**, *66*, 43403.

(38) Bandrauk, A. D.; Chelkowski, S. LIED: Laser induced electron diffraction by intense laser−molecule interaction—An exact non-Born−Oppenheimer simulation of the one-electron system: H_2^+. *J. Mol. Struct. (THEOCHEM)* **2002**, *591*, 199.

(39) Bandrauk, A. D.; Chelkowski, S.; Kawata, I. Molecular above-threshold-ionization spectra: The effect of moving nuclei. *Phys. Rev. A* **2003**, *67*, 13407.

(40) Bandrauk, A. D.; Lu, H. Z. Laser-induced electron recollision in H_2 and electron correlation. *Phys. Rev. A* **2005**, *72*, 23408.

(41) Bandrauk, A. D.; Lu, H. Z. Harmonic generation in a 1D model of H_2 with single and double ionization. *J. Phys. B* **2005**, *38*, 2529.

(42) Kamta, G. L.; Bandrauk, A. D. Three-dimensional time-profile analysis of high-order harmonic generation in molecules: Nuclear interferences in H_2^+. *Phys. Rev. A* **2005**, *71*, 53407.

(43) Kamta, G. L.; Bandrauk, A. D. Three-dimensional analysis of nuclear contributions to harmonic generation in H_2^+. *Laser Phys.* **2005**, *15*, 502.

(44) Nguyen, N. A.; Bandrauk, A. D. Electron correlation of one-dimensional H_2 in intense laser fields: Time-dependent extended Hartree−Fock and time-dependent density-functional-theory approaches *Phys. Rev. A* **2006**, *73*, 32708.

(45) Bandrauk, A. D.; Lu, H. Z. Electron correlation and double ionization of a 1D H_2 in an intense laser field. *J. Mod. Opt.* **2006**, *53*, 35.

(46) Bandrauk, A. D.; Barmaki, S.; Kamta, G. L. Laser phase control of high-order harmonic generation at large internuclear distance: The H^+−H_2^+ system. *Phys. Rev. Lett.* **2007**, *98*, 13001.

(47) Usachenko, V. I.; Pyak, P. E.; Chu, S. I. High-order harmonic generation in laser-irradiated homonuclear diatomics: The velocity gauge version of the molecular strong-field approximation. *Laser Phys.* **2006**, *16*, 1326.

(48) Guan, X. X.; Tong, X. M.; Chu, S. I. Effect of electron correlation on high-order-harmonic generation of helium atoms in intense laser fields: Time-dependent generalized pseudospectral approach in hyperspherical coordinates. *Phys. Rev. A* **2006**, *73*, 23403.

(49) Chu, S. I. Recent development of self-interaction-free time-dependent density-functional theory for nonperturbative treatment of atomic and molecular multiphoton processes in intense laser fields. *J. Chem. Phys.* **2005**, *123*, 62207.

(50) Usachenko, V. I.; Chu, S. I. Strong-field ionization of laser-irradiated light homonuclear diatomic molecules: A generalized strong-field approximation−linear combination of atomic orbitals model. *Phys. Rev. A* **2005**, *71*, 63410.

(51) Telnov, D. A.; Chu, S. I. Ab initio study of high-order harmonic generation of H_2^+ in intense laser fields: Time-dependent non-Hermitian Floquet approach. *Phys. Rev. A* **2005**, *71*, 13408.

(52) Chu, X.; Chu, S. I. Role of the electronic structure and multielectron responses in ionization mechanisms of diatomic molecules in intense short-pulse lasers: An all-electron ab initio study. *Phys. Rev. A* **2004**, *70*, 61402.

(53) Chu, S. I.; Telnov, D. A. Beyond the Floquet theorem: Generalized Floquet formalisms and quasienergy methods for atomic and molecular multiphoton processes in intense laser fields. *Phys. Rep.* **2004**, *390*, 1.

(54) Greenman, L.; Ho, P. J.; Pabst, S.; Kamarchik, E.; Mazziotti, D. A.; Santra, R. Implementation of the time-dependent configuration-interaction singles method for atomic strong-field processes. *Phys. Rev. A* **2010**, *82*, 023406.

(55) Suzuki, M.; Mukamel, S. Charge and bonding redistribution in octatetraene driven by a strong laser field: Time-dependent Hartree−Fock simulation. *J. Chem. Phys.* **2003**, *119*, 4722.

(56) Suzuki, M.; Mukamel, S. Many-body effects in molecular photoionization in intense laser fields; time-dependent Hartree−Fock simulations. *J. Chem. Phys.* **2004**, *120*, 669.

(57) Kuleff, A. I.; Breidbach, J.; Cederbaum, L. S. Multielectron wave-packet propagation: General theory and application. *J. Chem. Phys.* **2005**, *123*, 44111.

(58) Breidbach, J.; Cederbaum, L. S. Migration of holes: Formalism, mechanisms, and illustrative applications. *J. Chem. Phys.* **2003**, *118*, 3983.

(59) Breidbach, J.; Cederbaum, L. S. Migration of holes: Numerical algorithms and implementation. *J. Chem. Phys.* **2007**, *126*, 034101.

(60) Kuleff, A. I.; Cederbaum, L. S. Charge migration in different conformers of glycine: The role of nuclear geometry. *Chem. Phys.* **2007**, *338*, 320.

(61) Lünnemann, S.; Kuleff, A. I.; Cederbaum, L. S. Ultrafast charge migration in 2-phenylethyl-*N*,*N*-dimethylamine. *Chem. Phys. Lett.* **2008**, *450*, 232.

(62) Hennig, H.; Breidbach, J.; Cederbaum, L. S. Electron correlation as the driving force for charge transfer: Charge migration following ionization in *N*-methyl acetamide. *J. Phys. Chem. A* **2005**, *109*, 409.

(63) Remacle, F.; Kienberger, R.; Krausz, F.; Levine, R. D. On the feasibility of an ultrafast purely electronic reorganization in lithium hydride. *Chem. Phys.* **2007**, *338*, 342.

(64) Remacle, F.; Levine, R. D. Charge migration and control of site selective reactivity: The role of covalent and ionic states. *J. Chem. Phys.* **1999**, *110*, 5089.

(65) Remacle, F.; Levine, R. D. The time scale for electronic reorganization upon sudden ionization of the water and water−methanol hydrogen bonded dimers and of the weakly bound NO dimer. *J. Chem. Phys.* **2006**, *125*, 133321.

(66) Remacle, F.; Levine, R. D. An electronic time scale in chemistry. *Proc. Natl. Acad. Sci. U.S.A.* **2006**, *103*, 6793.

(67) Remacle, F.; Levine, R. D. Probing Ultrafast Purely Electronic Charge Migration in Small Peptides. *Z. Phys. Chem.* **2009**, *221*, 647.

(68) Remacle, F.; Levine, R. D.; Ratner, M. A. Charge directed reactivity: A simple electronic model, exhibiting site selectivity, for the dissociation of ions. *Chem. Phys. Lett.* **1998**, *285*, 25.

(69) Remacle, F.; Nest, M.; Levine, R. D. Laser Steered Ultrafast Quantum Dynamics of Electrons in LiH. *Phys. Rev. Lett.* **2007**, *99*, 183902.

(70) Nest, M.; Klamroth, T.; Saalfrank, P. The multiconfiguration time-dependent Hartree−Fock method for quantum chemical calculations. *J. Chem. Phys.* **2005**, *122*, 124102.

(71) Krause, P.; Klamroth, T. Dipole switching in large molecules described by explicitly time-dependent configuration interaction. *J. Chem. Phys.* **2008**, *128*, 234307.

(72) Krause, P.; Klamroth, T.; Saalfrank, P. Molecular response properties from explicitly time-dependent configuration interaction methods. *J. Chem. Phys.* **2007**, *127*, 034107.

(73) Krause, P.; Klamroth, T.; Saalfrank, P. Time-dependent configuration-interaction calculations of laser-pulse-driven many-electron dynamics: Controlled dipole switching in lithium cyanide. *J. Chem. Phys.* **2005**, *123*, 74105.

(74) Klamroth, T. Optimal control of ultrafast laser driven many-electron dynamics in a polyatomic molecule: *N*-Methyl-6-quinolone. *J. Chem. Phys.* **2006**, *124*, 144310.

(75) Tremblay, J. C.; Krause, P.; Klamroth, T.; Saalfrank, P. Time-dependent response of dissipative electron systems. *Phys. Rev. A* **2010**, *81*, 063420.

(76) Tremblay, J. C.; Klamroth, T.; Saalfrank, P. Time-dependent configuration-interaction calculations of laser-driven dynamics in presence of dissipation. *J. Chem. Phys.* **2008**, *129*, 084302.

(77) Klinkusch, S.; Saalfrank, P.; Klamroth, T. Laser-induced electron dynamics including photoionization: A heuristic model within time-dependent configuration interaction theory. *J. Chem. Phys.* **2009**, *131*, 114304.

(78) Liang, W. K.; Isborn, C. M.; Li, X. S. Laser-Controlled Dissociation of $C_2H_{22}^+$: Ehrenfest Dynamics Using Time-Dependent Density Functional Theory. *J. Phys. Chem. A* **2009**, *113*, 3463.

(79) Liang, W.; Isborn, C. M.; Lindsay, A.; Li, X. S.; Smith, S. M.; Levis, R. J. Time-Dependent Density Functional Theory Calculations of Ehrenfest Dynamics of Laser Controlled Dissociation of NO^+: Pulse Length and Sequential Multiple Single-Photon Processes. *J. Phys. Chem. A* **2010**, *114*, 6201.

(80) Li, X. S.; Tully, J. C.; Schlegel, H. B.; Frisch, M. J. Ab initio Ehrenfest dynamics. *J. Chem. Phys.* **2005**, *123*, 084106.

(81) Li, X. S.; Smith, S. M.; Markevitch, A. N.; Romanov, D. A.; Levis, R. J.; Schlegel, H. B. A time-dependent Hartree−Fock approach for studying the electronic optical response of molecules in intense fields. *Phys. Chem. Chem. Phys.* **2005**, *7*, 233.

(82) Smith, S. M.; Li, X. S.; Markevitch, A. N.; Romanov, D. A.; Levis, R. J.; Schlegel, H. B. A numerical simulation of nonadiabatic electron excitation in the strong field regime: Linear polyenes. *J. Phys. Chem. A* **2005**, *109*, 5176.

(83) Smith, S. M.; Li, X. S.; Markevitch, A. N.; Romanov, D. A.; Levis, R. J.; Schlegel, H. B. Numerical simulation of nonadiabatic electron excitation in the strong field regime. 2. Linear polyene cations. *J. Phys. Chem. A* **2005**, *109*, 10527.

(84) Smith, S. M.; Li, X.; Markevitch, A. N.; Romanov, D. A.; Levis, R. J.; Schlegel, H. B. A Numerical Simulation of Nonadiabatic Electron Excitation in the Strong-Field Regime: 3. Polyacene Neutrals and Cations. *J. Phys. Chem. A* **2007**, *111*, 6920.

(85) Smith, S. M.; Romanov, D. A.; Li, X. S.; Sonk, J. A.; Schlegel, H. B.; Levis, R. J. Numerical Bound State Electron Dynamics of Carbon Dioxide in the Strong-Field Regime. *J. Phys. Chem. A* **2010**, *114*, 2576.

(86) Smith, S. M.; Romanov, D. A.; Heck, G.; Schlegel, H. B.; Levis, R. J. Observing the Transition from Stark-Shifted, Strong-Field Resonance to Nonadiabatic Excitation. *J. Phys. Chem. C* **2010**, *114*, 5645.

(87) Caricato, M.; Trucks, G. W.; Frisch, M. J.; Wiberg, K. B. Electronic Transition Energies: A Study of the Performance of a Large Range of Single Reference Density Functional and Wave Function Methods on Valence and Rydberg States Compared to Experiment. *J. Chem. Theory Comput.* **2010**, *6*, 370.

(88) Schreiber, M.; Silva-Junior, M. R.; Sauer, S. P. A.; Thiel, W. Benchmarks for electronically excited states: CASPT2, CC2, CCSD, and CC3. *J. Chem. Phys.* **2008**, *128*, 134110.

(89) Frisch, M. J.; Trucks, G. W.; Schlegel, H. B.; Scuseria, G. E.; Robb, M. A.; Cheeseman, J. R.; Montgomery, J. A., Jr.; Vreven, T.; Kudin, K. N.; Burant, J. C.; Millam, J. M.; Iyengar, S.; Tomasi, J.; Barone, V.; Mennucci, B.; Cossi, M.; Scalmani, G.; Rega, N.; Petersson, G. A.; Nakatsuji, H.; Hada, M.; Ehara, M.; Toyota, K.; Fukuda, R.; Hasegawa, J.; Ishida, M.; Nakajima, T.; Honda, Y.; Kitao, O.; Nakai, H.; Klene, M.; Li, X.; Knox, J. E.; Hratchian, H. P.; Cross, J. B.; Bakken, V.; Adamo, C.; Jaramillo, J.; Gomperts, R.; Stratmann, R. E.; Yazyev, O.; Austin, A. J.; Cammi, R.; Pomelli, C.; Ochterski, J.; Ayala, P. Y.; Morokuma, K.; Voth, G. A.; Salvador, P.; Dannenberg, J. J.; Zakrzewski, V. G.; Dapprich, S.; Daniels, A. D.; Strain, M. C.; Farkas, Ö.; Malick, D. K.; Rabuck, A. D.; Raghavachari, K.; Foresman, J. B.; Ortiz, J. V.; Cui, Q.; Baboul, A. G.; Clifford, S.; Cioslowski, J.; Stefanov, B. B.; Liu, G.; Liashenko, A.; Piskorz, P.; Komaromi, I.; Martin, R. L.; Fox, D. J.; Keith, T.; Al-Laham, M. A.; Peng, C. Y.; Nanayakkara, A.; Challacombe, M.; Gill, P. M. W.; Johnson, B.; Chen, W.; Wong, M. W.; Gonzalez, C.; Pople, J. A. *Gaussian Development Version H10*; Gaussian, Inc.: Pittsburgh, PA, 2010.

(90) *Mathematica 5.0*; Wolfram Research, Inc.: Champaign, IL, 2003.

(91) Lias, S. G. Ionization Energy Evaluation. In *NIST Chemistry WebBook*; NIST Standard Reference Database Number 69; National Institute of Standards and Technology: Gaithersburg, MD, 2010.